



Research

Effects of Carrier Supply to the Intermediate Band by Impurity Doping on Two-Step Photocurrent Generation in GaAs:N-Based Intermediate Band Solar Cell

Md Faruk Hossain^{1, 2*}, Shuhei Yagi¹, Hiroyuki Yaguchi¹

¹Graduate School of Science and Engineering, Saitama University, Saitama 338-8570, Japan ²Department of Physics, Rajshahi University of Engineering & Technology, Rajshahi 6204, Bangladesh

Abstract: This study investigates the enhancement of two-step photocurrent generation in GaAs:N-based intermediate band solar cells (IBSCs) by optimizing the doping concentrations within the absorber layer. Utilizing the combination of device simulations and rate equation analysis, we examine the influence of doping levels of absorber on the key photovoltaic parameters and expected current increase due to two-step photon absorption. The results reveal that increasing the doping concentration enhances the number of electrons occupying the intermediate band (IB). Those electrons contribute to the low-energy photon absorption and the following additional current generation. However, the doping simultaneously reduced open-circuit voltage and fill factor due to the weakened electrical isolation of the IB from the contact layer. The expected efficiency gain due to the two-step photocurrent generation is unfortunately too small to compensate the drop in the base efficiency in the investigated structures. However, these results suggest that carrier supply to the IB states by means of impurity doping can be an effective option for structural optimization of IBSCs. These findings underscore the importance of carefully tuning the doping levels to maximize the efficiency of IBSCs and provide critical insights for the design of next-generation solar cells.

Keywords: Intermediate Band Solar Cells, Dilute Nitride Alloys, Two-Step Photocurrent Generation, Device Simulation, Rate Equation Analysis

*Corresponding Author

Accepted: 09 February, 2025; Published: 21 February, 2025

How to cite this article: Md Faruk Hossain, Shuhei Yagi, Hiroyuki Yaguchi (2025). Effects of Carrier Supply to the Intermediate Band by Impurity Doping on Two-Step Photocurrent Generation in GaAs:N-Based Intermediate Band Solar Cell. North American Academic Research, 8(2), 112-128. doi: https://doi.org/10.5281/zenodo.14910609

Conflicts of Interest: There are no conflicts to declare.

Publisher's Note: NAAR stays neutral about jurisdictional claims in published maps/image and institutional affiliations.

Copyright: ©2024 by the authors. Author(s) are fully responsible for the text, figure, data in this manuscript submitted for possible open access publication under the terms and conditions of the Creative Commons Attribution (CC BY) license (https://creativecommons.org/licenses/by/4.0/).

Introduction

One of the emerging third-generation solar cell concepts, the intermediate band solar cell (IBSC) has drawn extensive research attention because of its potential of exceeding the Shockley-Queisser efficiency limit of conventional single-gap solar cells (Luque et al. 1997; Green et al. 2002; Okada et al. 2015; Ramiro el al. 2021). In IBSC, two-step photocurrent is generated by the sequential absorption of below-bandgap photons in the light absorber semiconductor with the help of intermediate-band (IB) which exists between the valence band (VB) and conduction band (CB), leading to an increase

in the output current and thus contributing to the enhancement in the conversion efficiency of the solar cell. This concept is particularly advantageous for next-generation high-efficiency solar cells, where maximizing the utilization of the solar spectrum is essential for achieving performance beyond conventional single-junction photovoltaics. The selection of an appropriate absorber layer is crucial for effective IBSC operation. A dilute nitride semiconductor alloy, GaAs:N, is one of the most promising absorber layer materials for the operation of IBSC because of its distinctive band structure (Shan et al. 2000; O'Reillay et al. 2004; Noguchi et al. 2013; Polak et al. 2019). The integration of a small percentage of nitrogen into GaAs (resulting in GaAs:N) leads to splitting the CB into two non-parabolic subbands with energy minima at E- and E+. It has been demonstrated that using these conduction subbands is an effective strategy for composing an IB material in which E- and E+ bands are used as IB and CB, respectively (López et al. 2011; Ahsan et al. 2012; Ahsan et al. 2015; Suzuki el al. 2015; Jussila et al. 2015; Ahsan et al. 2022; Yagi el al. 2023). This band splitting enhances subbandgap photon absorption, making GaAs:N a highly promising material for IBSCs. In an effective IBSC, IB needs to be electrically isolated and optically connected with the VB and CB to avoid a voltage drop. This means that the optical transition should be the only way to couple the IB with the VB and CB (Antolín et al. 2010; Marti et al. 2012). This condition is crucial to prevent unwanted carrier leakage that could reduce the efficiency of the device. In prototype IBSCs with a GaAs:N absorber reported so far, these conditions were achieved by inserting a material such as AlGaAs between the absorber and contact layers, which has a band gap larger than the subgap energies (i.e. > the CB-IB gap and IB-VB gap, typically close to the CB-VB gap) of the absorber layer material. Such an electron blocking layer (EBL) facilitates selective collection of carriers from the VB and CB while not from the IB, and a resultant improvement in the carrier collection by the two-step photocurrent generation process was demonstrated in GaAs:N based IBSCs (López et al. 2011; Ahsan et al. 2012; Ahsan et al. 2015; Suzuki el al. 2015; Jussila et al. 2015; Ahsan et al. 2022; Yagi el al. 2023). However, the current increase of practical magnitude that could contribute to a conversion efficiency enhancement has not yet been achieved, and thus further optimization of the device structure is essential.

In an attempt to propose more effective semiconductor device designs, it is crucial to gain a thorough understanding of their operation and to optimize the doping, thickness and material properties of each layer in the device structure. Achieving an optimal balance between these parameters can significantly influence carrier dynamics, recombination rates, and overall photovoltaic performance. Device simulation plays a pivotal role in this process. Several models have been developed to simulate IBSC operation by incorporating an extra band in the CB-VB gap. These models, especially for quantum-dot-based IBSCs, provide valuable insights, though most are not open-source, with Simdo being an exception (Tobías et al. 2010; Wang et al. 2014; Strandberg et al. 2011; Lin et al. 2009; Yoshida et al. 2012; Dumitrescu et al. 2020). While standard commercial software typically cannot handle IBs, it remains valuable for IBSC analysis due to its extensive physical models and user-friendly interface. In a previous research, we established a technique to analyze the two-step photocurrent generation process in IBSCs through a combination of numerical device simulation and rate equation analysis (Hossain et al. 2025). In order to check the validity of the proposed methods, we applied it to an IBSC having a GaAs:N IB absorber with the same layered structure as the one experimentally investigated (Yagi el al. 2023). As a result, it was demonstrated that experimentally observed IBSC characteristics such as the voltage-dependent current increase through the two-step photocurrent generation process induced by below-gap photon excitation were well reproduced. The analytical results provided us various insights into device parameters in its operating states, thereby enabling a better understanding of device physics and effective structural design. For example, it was implied that one reason for a tiny current gain in the two-step photocurrent generation process was insufficient electron density occupying the IB states at the operating bias condition. The IB states have roles both to accept electrons excited from the VB and to accumulate electrons for absorbing low-energy photons which contribute to current after excitation to the CB. Therefore, half-filled IB stated is ideally required for an efficient IBSC operation (Luque et al. 2006). The IB occupancy is practically controllable by impurity doping (Okada et al. 2011). As the doping will change the built-in internal field in the device at the same time, careful design considering the balance of each effect is required. In this current study, we focus on exploring the effects of impurity doping in the absorber layer on the two-step photocurrent generation in GaAs:N-based IBSCs by utilizing the analytical method developed in Ref. (Hossain et al. 2025), and discuss the optimal structural design toward highly efficient IBSCs.

Research Methodology

A. Analytical Approach for Evaluating the Two-Step Photocurrent Generation Process

To assess IBSCs, external quantum efficiency (EQE) under monochromatic light is typically measured, revealing electron response in energies lower than the CB-VB gap but higher than the IB-VB gap (Ahsan et al. 2012; Sujuki et al. 2015; Jussila et al. 2015; Yagi et al. 2023; Antolín et al. 2010). This implies that electrons in the IB are transported to the contact layers via non-optical mechanisms, including thermal escape and field-assisted tunneling. In GaAs:N, rapid relaxation of electrons from the E_{+} to E_{-} band limits direct transport to the contacts, suggesting that IBSC behavior resembles a conventional semiconductor with an IB-VB gap in steady state. The two-step photocurrent generation—a key process in IBSC operation—is assessed by comparing the photocurrent (J) with and without the addition of low-energy photons that excite electrons from the IB to the CB. The resulting change in J (ΔJ), usually minor, confirms the contribution of low-energy photons, although the impact on electron distribution remains modest. To estimate ΔJ , simulations treat the GaAs:N absorber as a conventional single-gap material, calculating device outputs and then estimating current increases based on rate equations under low-energy photon illumination.

B. Device Structure and Simulation Parameters

To investigate the doping effects, we start with the device structure illustrated in Fig. 1(a). The corresponding band diagram in the equilibrium condition is shown in Fig. 1(b). This IBSC structure is identical to that prepared in the experiments described in Ref. (Yagi et al. 2023) and that analyzed in Ref. (Hossain et al. 2025). The layered configuration from top to bottom includes eight distinct layers. The schematic structure contains the details of the name, thickness and doping concentration of each layer. A GaAs:N layer without intentional carrier doping is placed between p- and nlayers as the optical absorber. It was confirmed in Ref. (Yagi et al. 2023) that the conduction subbands of E- and E+ were formed in this layer at 1.15 eV and 1.50 eV above the VB edge, respectively. The Al composition of 0.15 in the AlGaAs EBL adjacent to the absorber creates barriers of 0.42 eV for the electrons in the IB states and 0.07 eV for those in the CB states in the GaAs:N absorber at the interface. A part of the EBL is doped with n-type dopant whereas the other part of the EBL facing to the absorber is undoped. Device simulation was carried out by using a commercial software, Silvaco ATLAS to obtain conventional photovoltaic characteristics such as *EQE* and current density versus voltage (*J-V*) curves. In the simulation, the GaAs:N absorber was treated as a conventional single-gap material with a bandgap of 1.15 eV equivalent to the IB (E-) -VB gap. The dielectric function spectrum of GaAs:N was given based on the model dielectric function formulated in Ref. (Leibiger et al. 2001). According to the previous studies (Ishikawa et al. 2005; Reason et al. 2007; Umeno et al. 2010), the mobilities for electrons and holes in the GaAs:N region were set at 2×10² and 1×10² cm²/(Vs), respectively. An acceptor-like trap at 0.45 eV below the IB edge with a density of 8.0×10¹⁷ cm⁻³ was introduced in the GaAs:N absorber as it was necessary to reproduce the experimental results (Hossain et al. 2025). The interface recombination velocities were also adjusted as described in Fig. 1(a) so that the experimental results are reproduced. The formulas obtained from Ref. (NSM Archive) were used to calculate the energy band gap and electron affinity of AlxGa1-xAs layers. The Silvaco ATLAS default values were assigned to other material parameters (ATLAS User's Manual, 2022). Then we studied different structures in which n-type doping was applied to the GaAs:N absorber with various doping concentrations to see the impact of the doping on the device behavior. To observe the carrier dynamics regarding to the IB states, response to the light illumination at a wavelength of 980 nm was calculated. Photons at this wavelength are absorbed only in the GaAs:N absorber layer, so it is expected to elucidate the carrier escape process from the

absorber. In addition to that, we employed AM1.5G solar radiation as the source of illumination to discuss the effects on the power generation performance of the solar cells under practical conditions.

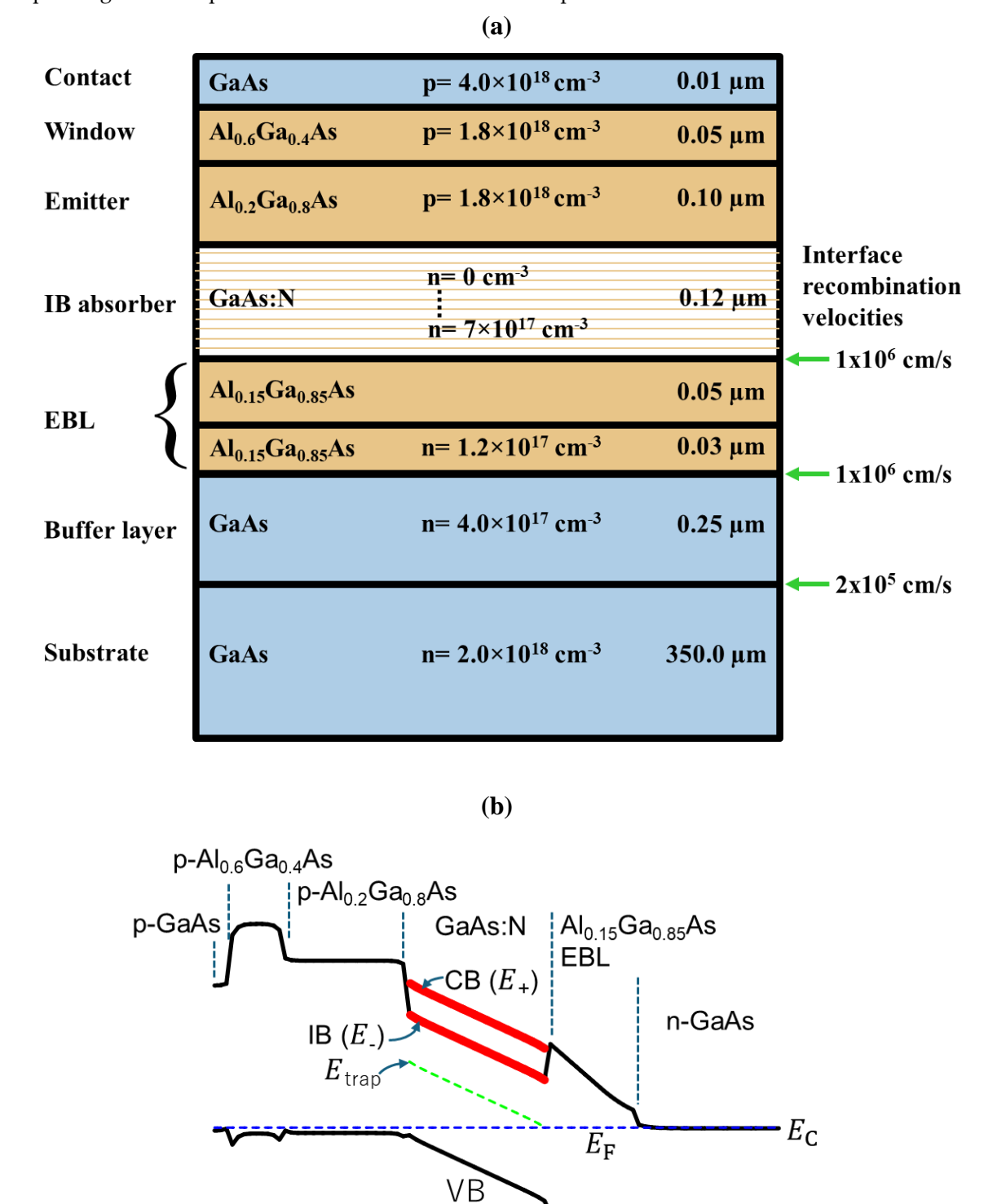


Fig. 1: (a) Schematic device structure and, (b) band diagram in the equilibrium condition of the IBSC analyzed in this study.

 $\cdot E_{
m V}$

C. Two-Step Photocurrent Generation Analysis by Rate Equation

The process of generating photocurrent through two-step photon absorption was examined using a rate equation model, incorporating parameters derived from device simulations. This analysis considers the photocurrent generation mechanism in the IB absorber with two distinct contributions of the illumination light source: one that promotes electron transitions from the VB to the IB and the other that facilitates transitions from the IB to the CB within the IB absorber. For the GaAs:N IB absorber layer, the rate equation can be written as,

$$\frac{dn_{\rm CB}}{dt} = G_{\rm CI} - R_{\rm CI} - \frac{J_{\rm CB}}{e} \tag{1}$$

$$\frac{dn_{\rm IB}}{dt} = G_{\rm IV} - G_{\rm CI} - R_{\rm IV} + R_{\rm CI} - \frac{J_{\rm IB}}{e} \tag{2}$$

In this context, n_{CB} and n_{IB} represent the sheet electron densities in the CB and IB, respectively within the absorber region. The symbol G signifies the generation rate, while R represents the recombination rate. The subscripts CI and IV refer to the transitions of CB-IB and IB-VB, respectively. J_{CB} and J_{IB} are the current components contributed by the extraction of electrons in the CB and IB, respectively. Total current J is sum of these two current components, $J = J_{CB} + J_{IB}$. The generation rate G_{IV} depends on the flux density P_1 of the photons which have energy at least the IB-VB gap energy (E_{IV}). On the other hand, only photons with energy larger than the CB-IB gap (E_{CI}) and smaller than E_{IV} contribute to the rate of the IB to CB electron transition G_{CI} . For the illumination light source with the energy spectrum of the photon flux density p(E), the total photon flux densities of the second light source component P_2 is calculated as

$$P_2 = \int_{E_{CI}}^{E_{IV}} p(E) dE \tag{3}$$

 E_{CI} and E_{IV} have the values of 0.35 eV and 1.15 eV, respectively in this case. When the light source is the AM1.5G radiation, P_2 is calculated to be $1.62 \times 10^{17} \,\text{s}^{-1}\text{cm}^{-2}$. This value is used in the analysis shown in a later section. As a result of solving the above equations (1) and (2) at the steady state, current increase ΔJ induced by the second light source component, in other words, the contribution of the two-step photocurrent generation, is derived as follows (please refer to the appendix and Ref. (Hossain et al. 2025) for the detailed derivation):

$$\Delta J = e(1 - CCE)n_{\rm IB} \frac{f_{\rm CB}\sigma}{\gamma_{\rm CI} + f_{\rm CB}} P_2, \tag{4}$$

where γ_{CI} , f_{CB} and σ are the inverse lifetime of the CB electrons for relaxation to the IB states, the extraction rate of the CB electrons to the n-type contact layer through the EBL, and the absorption cross-section of the electrons in the IB states, respectively. These three parameters are determined by the material properties and device structure. The factor $f_{CB}\sigma/(\gamma_{CI}+f_{CB})$ was estimated to be 3.47×10^{-11} cm² from the comparison with experimental results for the device under analysis (Yagi et al. 2023; Hossain et al. 2025). In the present analysis, we fix this value as a factor independent of the doping concentration in the GaAs:N absorber. So, the equation (4) suggests that we need to look for conditions such that the factor $(1-CCE)n_{IB}$ becomes large as much as possible to obtain large current gain induced by the two-step photocurrent generation process. CCE is the carrier collection efficiency (Fujii et al. 2012), defined as the proportion of carriers contributing to the photocurrent relative to the total photo-generated carriers in the absorber potentially available. This factor strongly depends on the bias voltage and is easily estimated from the J-V curve under photo-illumination as $CCE = J/J_{Sat}$, where J_{Sat} is the saturation photocurrent density under sufficiently large reverse bias. We calculated CCE and n_{IB} based on the results of the device simulation and used them as input parameters to deduce ΔJ from equation (4). The factor (1-CCE) in equation (4) reflects the requirement of electrical isolation of the IB. If

photogenerated electrons in the IB states are evacuated to the contact layer without the help of IB-CB photoexcitation, *CCE* becomes close to unity and ΔJ drastically decrease. The sheet density of the IB electrons in the GaAs:N absorber $n_{\rm IB}$ was simply calculated by integrating the electron density distribution n(x) as follows:

$$n_{\rm IB} = \int_{\rm GaAs:N} n(x) \, dx,\tag{5}$$

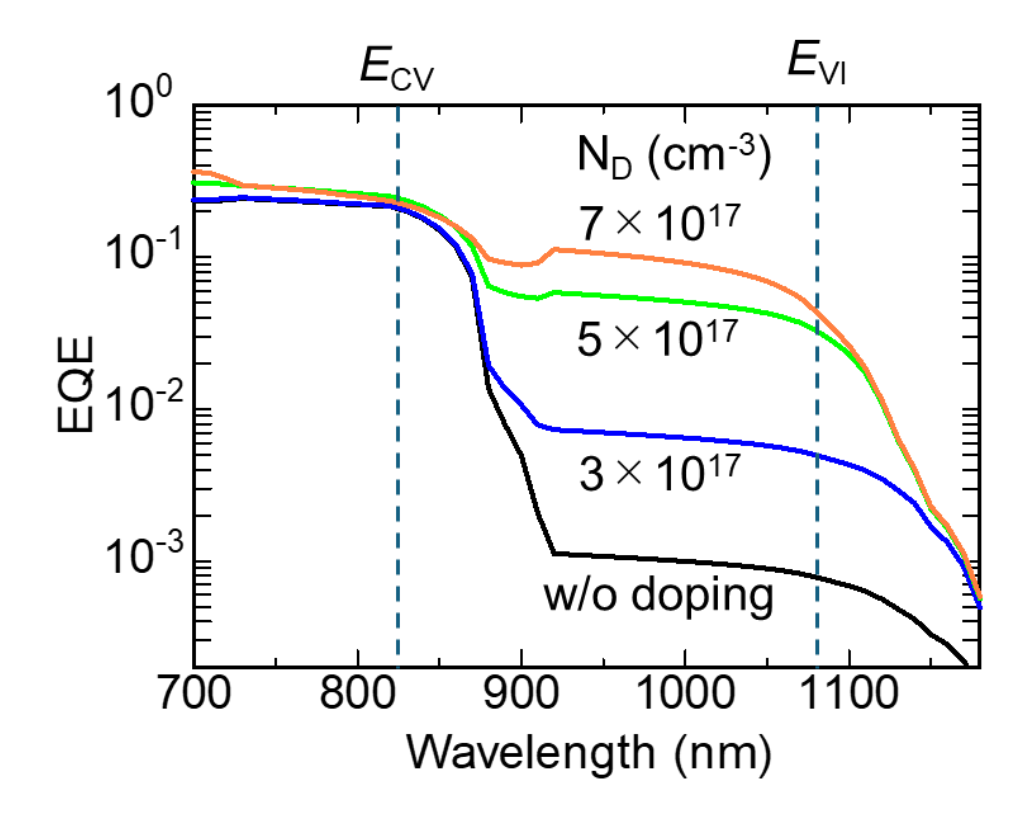
under the assumption that the density of the electron occupying the CB states is negligibly small compared with that of the IB states.

Results and Discussion

A. Effects of Doping Concentration in the Gaas:N Absorber Layer on the Carrier Extraction Process from the IB States

Fig. 2(a) depicts the simulation results of the EQE spectra at the short-circuit condition for GaAs:N-based IBSCs with various doping concentrations N_D in the absorber layer. The EQE in the energy range between the CB-VB gap (E_{CV}) and E_{IV} reflects the contribution of photocarriers generated by the VB to the IB transition. For the device without doping in the absorber, EQE significantly dropped for photon energies below E_{CV} in comparison with that for the shorter wavelength range, suggesting that the EBL effectively confines carriers within the IB level. As the doping concentration in the GaAs:N region increases, the EQE in this wavelength range increases, demonstrating the effect lessening electron confinement in the IB of the absorber region.

Fig. 2(b) shows the J-V curves of GaAs:N-based IBSCs with various doping concentrations in the GaAs:N absorber under the monochromatic light illumination at 980 nm with an intensity of 2 mW/cm². Photocarriers are generated only in the GaAs:N absorber at this excitation wavelength. Therefore, the J-V curves reflect the electron escape process from the IB in the GaAs:N layer. The current density converges to a certain value of about 0.16 mA/cm² as the reverse bias increases independently of the doping conditions, indicating all the photogenerated electrons in the IB states are extracted with the assistance of strong electric field. It is observed that the short circuit current density Jsc increases with increasing doping concentration as we also confirmed in the EQE spectra.



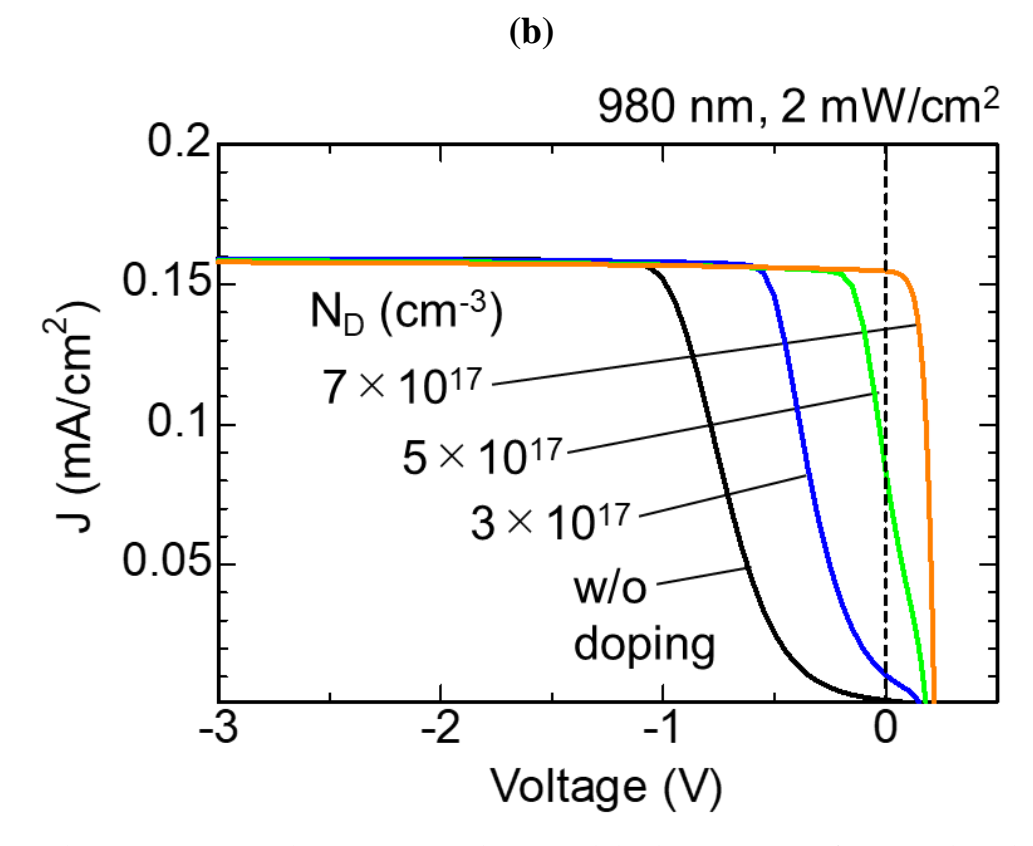


Fig. 2: (a) The *EQE* spectra at short-circuit condition, and (b) the *J-V* curves of GaAs:N-based IBSCs with various doping concentrations in the GaAs:N absorber.

CCE can be calculated based on the *J-V* curves, and Fig. 3 shows CCE at the short circuit condition as a function of N_D . Increase in N_D leads to a monotonical increase in the CCE and it reaches almost unity when N_D is over 6×10^{17} cm⁻³. This means that the EBL no longer serves to confine the photo-generated electrons in the IB, and thus the doping concentration should be less than that level to keep the electrical isolation of the IB.

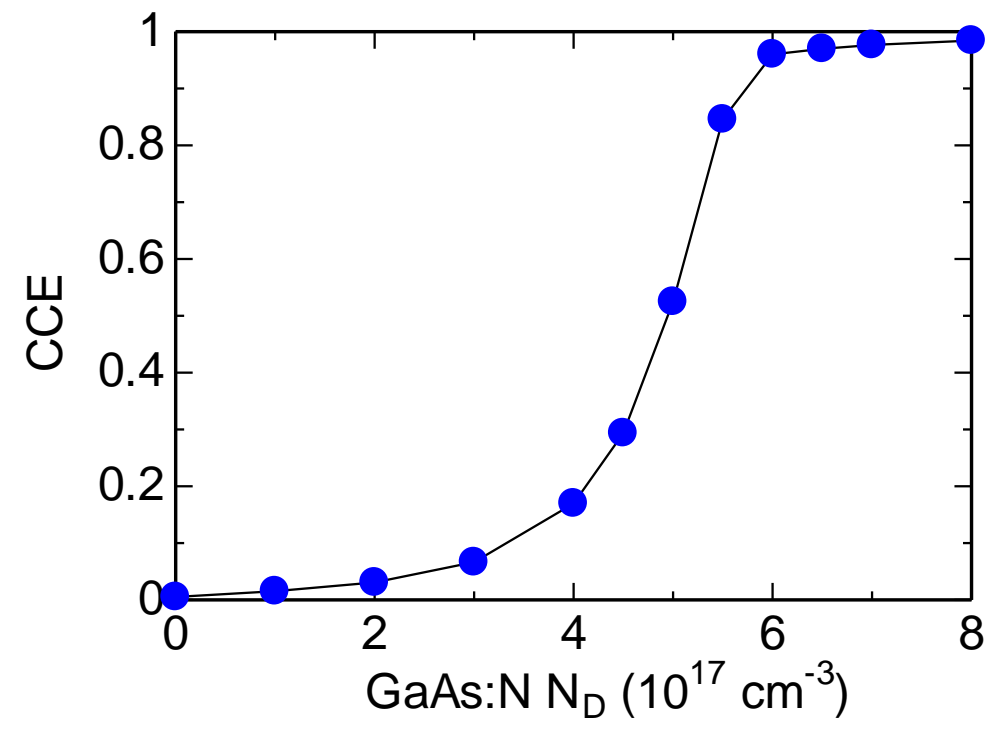


Fig. 3: The variation of CCE as a function of N_D at the short circuit condition.

Fig. 4 displays the energy band diagrams and electron concentration profiles in the vicinity of the absorber and EBL for GaAs:N-based IBSCs with varying doping concentrations in the GaAs:N absorber layer. The diagrams are presented under the same illumination condition as the results in Fig. 2(b) and 0 V bias voltage. It is seen from the band diagrams that the top of the EBL CB edge is lowered for the larger N_D . The weaker electron confinement effect of the EBL for the larger N_D is considered to originate from this change in the band profile. At the same time, the electron concentration at the interface between the absorber layer and EBL is enhanced with increasing doping concentration in the GaAs:N region due to electron supply from the dopants.

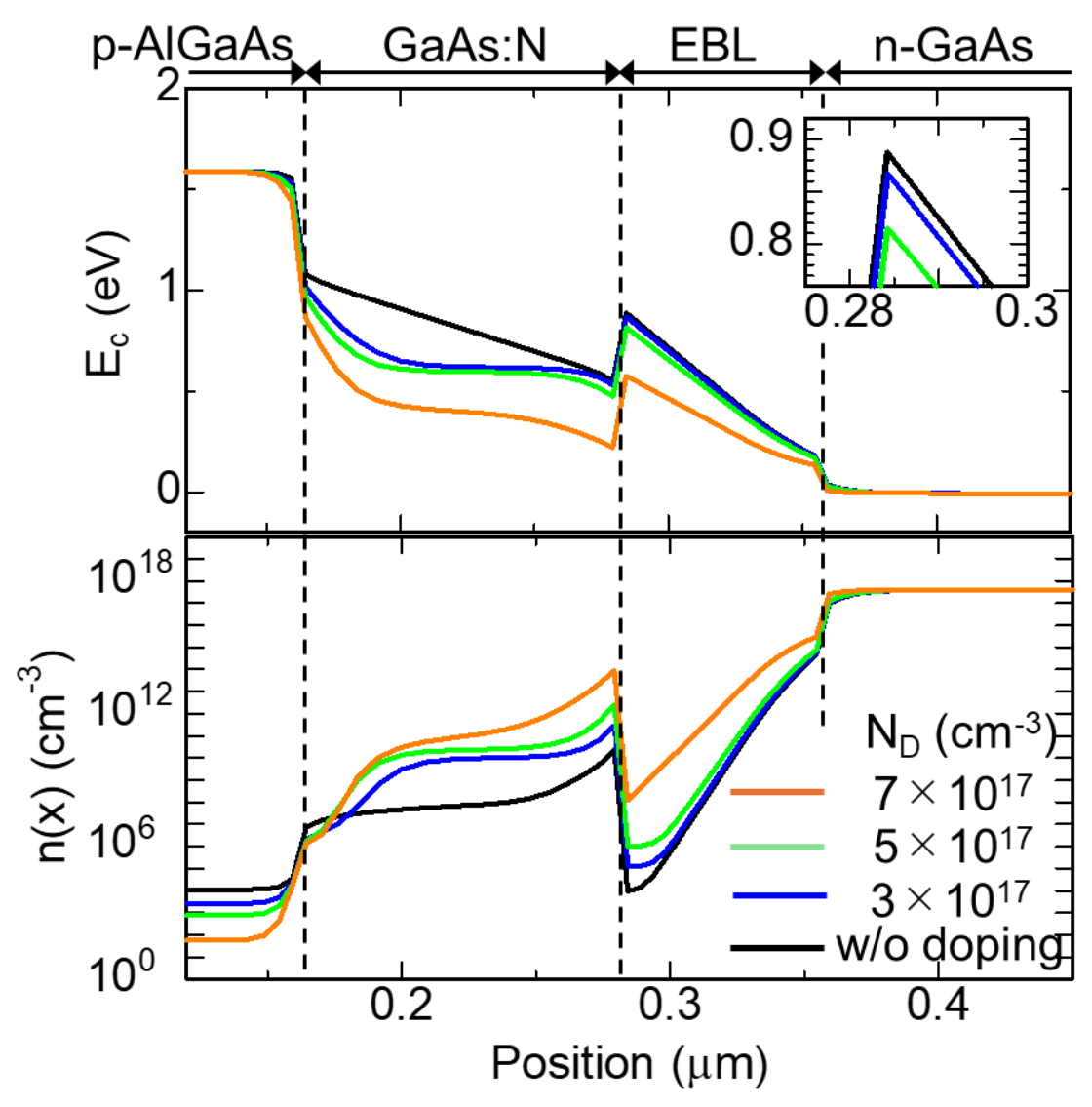


Fig. 4: The energy band diagrams (upper panel), and electron distribution profiles (lower panel) for GaAs:N-based IBSCs with different doping concentrations in the GaAs:N absorber layer.

The integrated electron concentration in the absorber region was calculated from these profiles as a function of $N_{\rm D}$, and the results are shown in Fig. 5(a) together with the factor (1-*CCE*). It can be seen that donor doping surely contributes to the increase in the number of electrons in the IB available for low-energy photon absorption. The factor (1-CCE) simultaneously increases with increasing $N_{\rm D}$, indicating the doping weakens electrical isolation of the IB required for the IBSC operation. Thus, the appropriate adjustment of the doping concentration is important. As mentioned above, the factor $(1-CCE)n_{\rm IB}$ is an essential parameter in the two-step photocurrent generation. The doping concentration dependence of this factor shown in Fig. 5(b) suggests that the donor doping in the GaAs:N absorber with the concentration of ~5×10¹⁷ cm⁻³ is considered to be an effective condition in terms of getting large current increment due to the two-step photocurrent generation process.

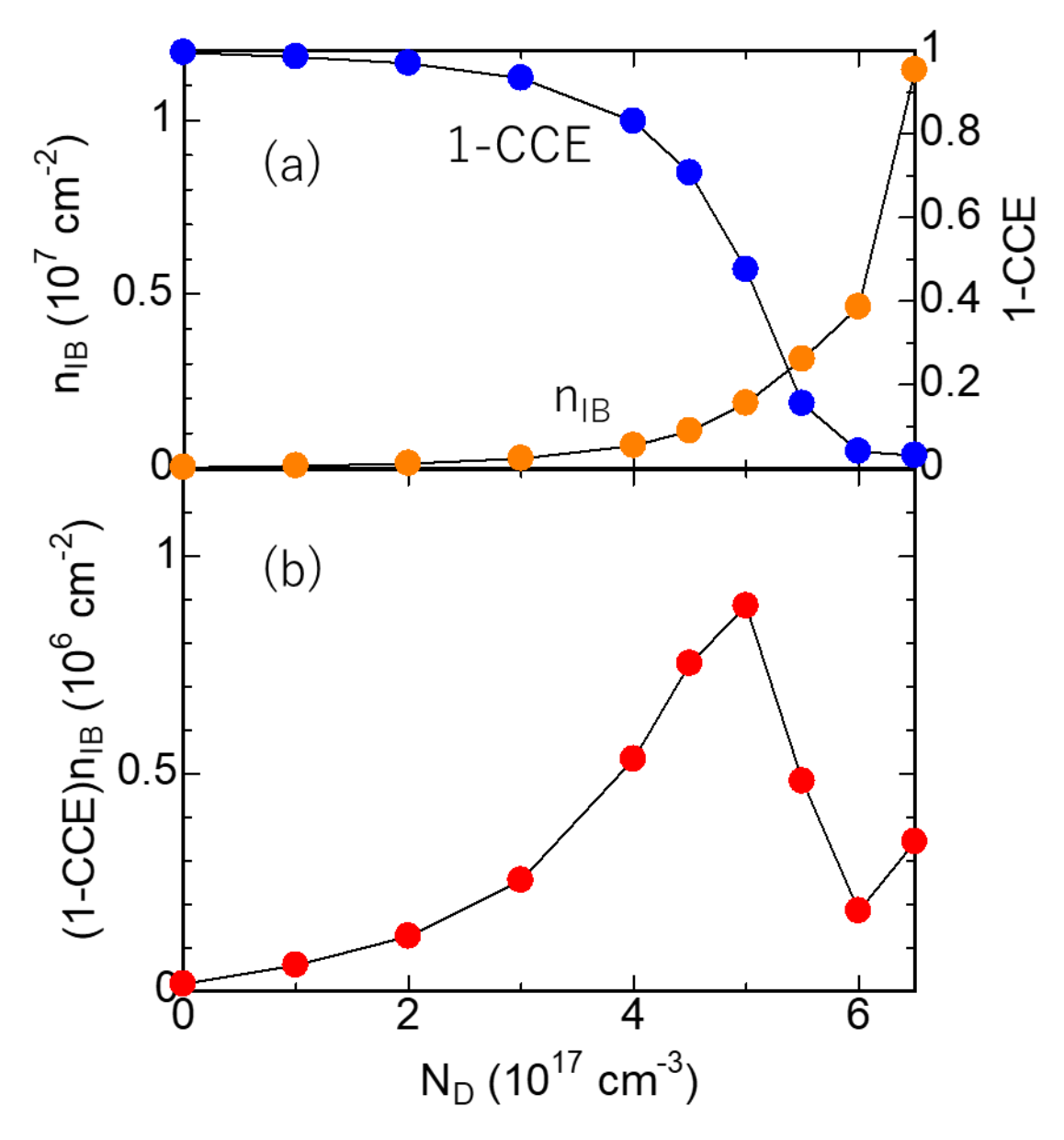


Fig. 5: The N_D dependence of (a) n_{IB} , (1 - CCE), and (b) $(1 - CCE)n_{IB}$ of GaAs:N-based IBSCs.

B. Analysis of Two-Step Photocurrent Generation under Sunlight Illumination

Fig. 6 shows J-V curves of GaAs:N-based IBSCs with various doping concentrations in GaAs:N region under AM1.5G illumination. It is observed that with increasing doping concentration in GaAs:N absorber layer, J_{SC} is increased owing to the weakened barrier effect of the EBL for the IB electrons as we have seen above. Simultaneously, the open circuit voltage (V_{CC}) and fill factor (FF) are reduced with increasing doping concentration in the GaAs:N absorber. The lowered barrier height of the EBL also leads to the larger forward current under forward bias which compensates for the photogenerated current and thus results in a reduction in both the V_{CC} and the FF. The cell with N_D of 7×10^{17} cm⁻³ which has an unblocked IB structure showed a significantly larger J_{SC} and smaller V_{CC} compared with the blocked IB structures similarly as found in other experimental works (O'Reilly et al. 2004; López et al. 2011). This unblocked IB cell is considered working as a simple pn junction cell composed of p-Alo₂Ga_{0.8}As and n-GaAs:N.

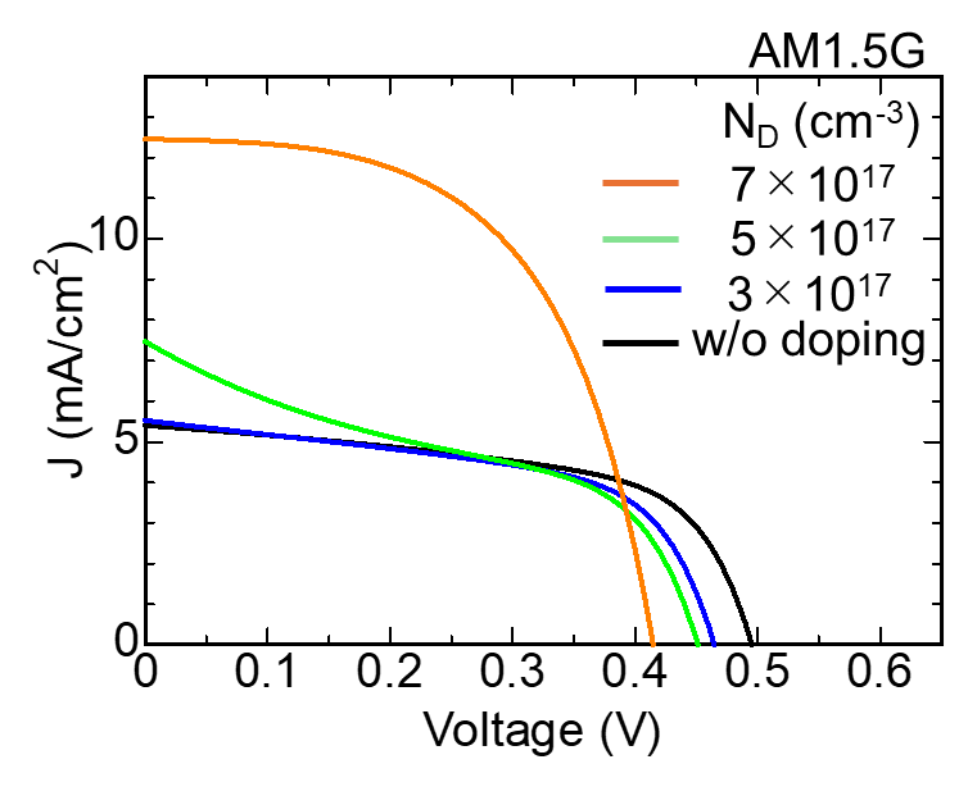


Fig. 6: J-V characteristics of GaAs:N-based IBSCs under AM1.5G illumination.

The variation of integrated electron concentration in the GaAs:N region with bias voltage under AM1.5G illumination is shown in Fig. 7 for three cells with blocked IB having different doping conditions in the absorber layer. The integrated electron concentration rises as the voltage changes from the positive to the negative applied voltage side, likely due to the reduction of carrier recombination caused by the spatial separation of electrons and holes in the stronger internal electric field induced in the absorber. It became maximum at a certain point and then it slightly decreased with the further increase in reverse bias voltage, owing to the increasing field-assisted extraction of electrons from the IB. The number of electrons in the IB with the larger doping concentration always keeps a larger value at any bias voltage.

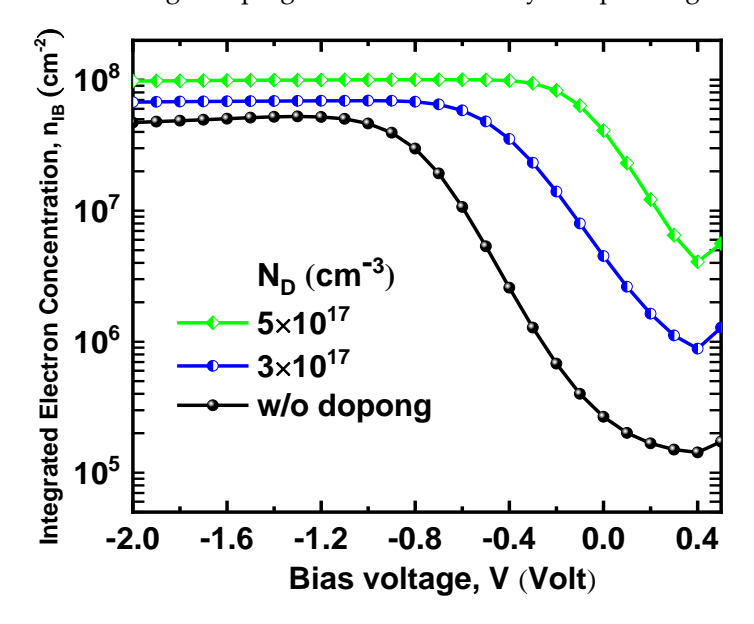


Fig. 7: The variation of integrated electron concentration in GaAs:N region with bias voltage under AM1.5G illumination.

The behavior of *CCE* is calculated from the *J-V* curves in Fig. 6 and the variation of the factor (1-*CCE*) as a function of the bias voltage is illustrated in Fig. 8, where it clearly shows that the onset voltage at which the factor(1-*CCE*) starts to rise shifts to the forward bias sides with increasing the doping concentration. This shift indicates that higher doping concentrations lead to a modification of the built-in electric field, potentially altering the charge separation dynamics within the device.

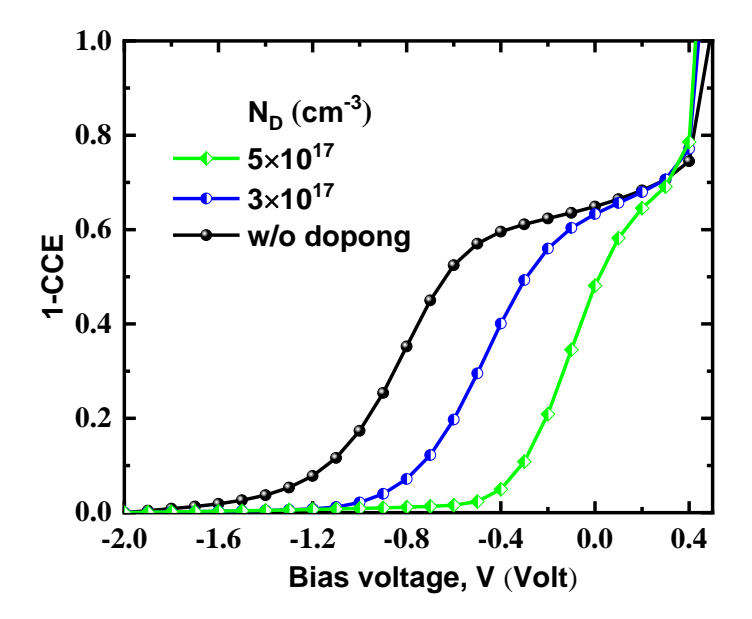


Fig. 8: The bias voltage dependence of (1-CCE) for different doping concentration of the GaAs:N absorber layer.

By utilizing equation (4) and the above data derived from the device simulation, we calculated voltage dependence of ΔJ as a metric for the expected current gain caused by the two-step photocurrent generation under sunlight illumination. The results are plotted in Fig. 9. A clear peak is observed in each $\Delta J - V$ curve originating from the voltage dependence of $n_{\rm IB}$ and (1 - CCE). The peak position is at -0.8 V for the cell with the undoped absorber and the magnitude of ΔJ is significantly small on the forward bias side compared with the peak value, meaning that the two-step photocurrent generation seldom contributes to enhancing the conversion efficiency in this IBSC. For the other doped structures, the peaks have higher amplitude and showed shifting towards the positive bias region. In particular, the solar cell with 5×10^{17} cm⁻³ doping concentration in the absorber layer has the ΔJ peak at a voltage close to the short circuit condition and non-negligible magnitude remains even around the maximum power operation point of ~0.35 V. In ref. (Yagi et al. 2023), the effect of the EBL barrier height changed by the Al composition on the two-step photocurrent generation process was investigated for the same structured devices as analyzed in this paper. It was observed there in ΔJ -V curves that the lowered EBL barrier caused a shift of ΔJ peak toward the positive voltage side similarly to this study. But differently from the results in Fig. 9, the peak height of ΔJ became significantly smaller with lowering the EBL barrier height because the lowered barrier weakened electron confinement and decreased electron density in the IB used to absorb low-energy photons. Table 1 summarizes the obtained photovoltaic parameters of the three investigated structures including the expected current and conversion efficiency gain caused by the two-step photocurrent generation. The current gains are shown for the short circuit condition and the maximum power point derived from the J-V curves. The base efficiency is decreased with increasing doping concentration in the absorber layer owing to the reduction of V_{oc} and FF. However, the highest increment in the efficiency of 1.2×10-3% is expected for the IBSC with 5×10¹⁷ cm⁻³ doping concentration in the absorber layer, whereas the undoped structure shows much smaller efficiency gain of 3.8×10⁻⁵% which is substantially negligible. This efficiency increment is unfortunately too small to compensate the drop in the base efficiency caused by the doping in the absorber in the investigated structures. However, these

results suggest that carrier supply to the IB states by means of impurity doping can be an effective option for structural optimization of IBSCs.

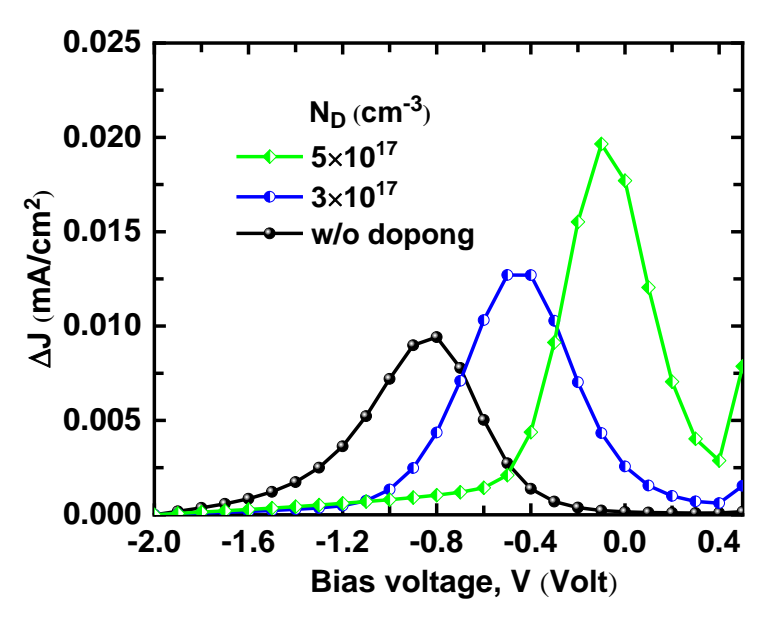


Fig. 9: The variation of ΔJ with bias voltage of the IBSCs.

Tuble 1. I efformative I drameters of 155 es.							
$N_{ m D}$	Performance Parameters						
(cm ⁻³)	$J_{\rm sc}$ (mA/cm ²)	ΔJ at the short circuit	ΔJ at the maximum	Voc (V)	FF	η	Δη
		condition (mA/cm²)	power point (mA/cm²)			(%)	(%)
w/o doping	5.40	1.6×10-4	9.5×10 ⁻⁵	0.488	0.595	1.579	3.8×10 ⁻⁵
3×10 ¹⁷	5.53	2.6×10-3	6.1×10-4	0.439	0.568	1.38	2.0×10-4
5×10 ¹⁷	7.50	1.8×10 ⁻²	4.0×10 ⁻³	0.428	0.418	1.34	1.2×10 ⁻³

Table 1: Performance Parameters of IBSCs.

Conclusion

This study systematically investigated the impact of varying doping concentrations in the GaAs:N absorber layer on the performance of GaAs:N-based IBSCs. By employing a combination of numerical device simulation and rate equation analysis, device states during the two-step photocurrent generation process were elucidated. Our results indicate that an n-type doping in the GaAs:N absorber layer supplies electrons occupying the IB states which can contribute to the current gain originating from two-step photon absorption. The optimal doping configuration leads to the highest efficiency gain, highlighting the importance of precise doping strategies in advancing IBSC technologies. However, the study also reveals that the increasing doping can detrimentally impact Voc and FF, as the decreased EBL barrier height enhances forward current under forward bias, offsetting the photo-generated current. The expected efficiency increment due to the two-step photocurrent generation is unfortunately too small to compensate the drop in the base efficiency in the investigated structures. However, these results suggest that carrier supply to the IB states by means of impurity doping can be an effective option for structural optimization of IBSCs. These insights provide a valuable framework for the design and development of more efficient IBSCs, contributing to the advancement of third-generation solar cell technologies.

APPENDIX

Derivation of Current Increment in Two-Step Photocurrent Generation Process by Rate Equation Model

The process of generating photocurrent through two-step photon absorption in an IBSC was examined using a rate equation model. This analysis considers the photocurrent generation mechanism under the illumination of two distinct light sources: one that promotes electron transitions from the VB to the IB and the other that facilitates transitions from the IB to the CB within the IB absorber. Experimentally, this condition can be realized by selecting a suitable wavelength combination of light sources λ_1 and λ_2 to satisfy

 $E_{\rm CV}/hc > \lambda_1 > E_{\rm CI}/hc$ and $E_{\rm IV}/hc > \lambda_2 > E_{\rm CI}/hc$.

For the IB absorber the rate equation can be written as,

$$\frac{dn_{\rm CB}}{dt} = G_{\rm CI} - R_{\rm CI} - \frac{J_{\rm CB}}{e} \tag{6}$$

$$\frac{dn_{\rm IB}}{dt} = G_{\rm IV} - G_{\rm CI} - R_{\rm IV} + R_{\rm CI} - \frac{J_{\rm IB}}{e},\tag{7}$$

In this context, n_{CB} and n_{IB} represent the electron densities in the CB and IB, respectively within the absorber region. The symbol G signifies the generation rate, while R represents the recombination rate. The subscripts CI and IV refer to the transitions of CB-IB and IB-VB, respectively.

 G_{CI} depends on both the intensity of the second light source and the electron density within the IB and can therefore be expressed by the following equation,

$$G_{\rm CI} = P_2 \sigma n_{\rm IB},\tag{8}$$

where σ and P_2 represent the absorption cross-section of electrons in the IB and the photon flux density of the second light source, respectively.

The recombination rate is a function of the inverse life time (γ) and can be expressed as,

$$R_{\rm IV} = \gamma_{\rm IV} n_{\rm IB} \tag{9}$$

$$R_{\rm CI} = \gamma_{\rm CI} n_{\rm CB} \tag{10}$$

Ideally, the IB is electrically isolated from the contact but in reality, a part of electrons in the IB can escape directly to the contact through thermal and/or tunneling effects. Here, the current contributions from both the CB and IB are considered with an assumption that they are in proportion to the electron density occupying each band and its extraction rate through the EBL. Thus, J_{CB} and J_{IB} , representing the current contributions of electrons in the CB and IB, respectively, can be defined by the following equations,

$$\frac{J_{\rm IB}}{e} = n_{\rm IB} f_{\rm IB} \tag{11}$$

$$\frac{J_{\rm CB}}{e} = n_{\rm CB} f_{\rm CB},\tag{12}$$

where f_{IB} is the extraction rates for an electron in the IB and f_{CB} is that in the CB.

The values of n_{CB} and n_{IB} are determined by solving the simultaneous equations (6)-(12) under steady-state conditions (i.e., when d/dt=0).

The total current density is obtained by summing the individual electron current components and can be calculated using the resulting equation,

$$J = J_{\rm CB} + J_{\rm IB} = eG_{\rm IV} \frac{f_{\rm CB}\sigma P_2 + f_{\rm IB}(\gamma_{\rm CI} + f_{\rm CB})}{(\gamma_{\rm IV} + f_{\rm IB} + \sigma P_2)(\gamma_{\rm CI} + f_{\rm CB}) - \gamma_{\rm CI}\sigma P_2}$$
(13)

The current component resulting from two-step photon absorption can be evaluated by measuring the increase in current density when a second light source is introduced to the system already illuminated by the first light source. Hence, the current increment ΔJ can be obtained by the equation given below,

$$\Delta J = J - J|_{P_2 = 0} = \frac{eG_{IV}\gamma_{IV}f_{CB}\sigma P_2}{\{(\gamma_{IV} + f_{IB} + \sigma P_2)(\gamma_{CI} + f_{CB}) - \gamma_{CI}\sigma P_2\}(\gamma_{IV} + f_{IB})}$$
(14)

The carrier collection efficiency (CCE) (Leibiger et al. 2001), defined as the proportion of carriers contributing to the current relative to the photo-generated carriers in the absorber, is determined by the balance between the rates of carrier extraction and recombination. Under illumination by only the first light source, CCE can be described by the following expression,

$$CCE = \frac{J_{\rm IB}}{eG_{\rm IV}} = \frac{f_{\rm IB}}{\gamma_{\rm IV} + f_{\rm IB}} \tag{15}$$

 ΔJ can be made simpler by applying the above form of CCE and n_{IB} as follows,

$$\Delta J = e(1 - CCE) \frac{f_{\text{CB}}\sigma}{\gamma_{\text{CI}} + f_{\text{CB}}} n_{\text{IB}} P_2$$
(16)

The change in J caused by the additional introduction of low-energy photon light source, denoted as ΔJ , is frequently utilized as a metric to assess two-step photocurrent generation.

Author Contributions: At first page.

Approval: All authors have read and agreed to the published version of the manuscript.

Funding: This research received no external funding.

Institutional Review Board Statement: Not applicable.

Informed Consent Statement: Not applicable.

Data Availability Statement: Not applicable

Acknowledgments: This work was supported in part by JSPS KAKENHI grant number JP22K04211.

Conflicts of Interest: The authors declare no conflict of interest.

References

- [1] Ahsan N, Miyashita N, Monirul Islam M., Man Yu K, Walukiewicz W, Okada Y. Two-photon excitation in an intermediate band solar cell structure. Applied Physics Letters, 2012; 100(17):172111.
- [2] Ahsan N, Miyashita N, Yu KM, Walukiewicz W, Okada Y. Electron barrier engineering in a thin-film intermediate-band solar cell. IEEE Journal of Photovoltaics, 2015; 5(3):878-884.
- [3] Ahsan N, Miyashita N, Yu KM, Walukiewicz W, Okada Y. Collection of photocarriers in intermediate band solar cells: experiments and equivalent circuit analysis. Journal of Photonics for Energy, 2022; 12(3):032210-032210.
- [4] Antolín E, Martí A, Farmer CD, Linares PG, Hernández E, Sánchez AM, Luque A. Reducing carrier escape in the InAs/GaAs quantum dot intermediate band solar cell. Journal of Applied Physics, 2010; 108(6).
- [5] ATLAS User's Manual, Device Simulation Software, SILVACO Inc., Santa Clara, 2022.
- [6] Dumitrescu EC, Wilkins MM, Krich JJ. Simudo: a device model for intermediate band materials. Journal of Computational Electronics, 2020; 19(1):111-127.
- [7] Fujii H, Watanabe K, Sugiyama M, Nakano Y. Effect of quantum well on the efficiency of carrier collection in InGaAs/GaAsP multiple quantum well solar cells. Japanese Journal of Applied Physics, 2012; 51(10S):10ND04.
- [8] Green MA. Third generation photovoltaics: solar cells for 2020 and beyond. Physica E: Low-dimensional Systems and Nanostructures, 2002; 14(1-2):65-70.
- [9] Hossain MF, Shuhei Y, Hiroyuki Y. Analysis of Two-Step Photocurrent Generation in GaAs:N-Based Intermediate Band Solar Cells with Utilization of Device Simulation. AIP Advances, 2025; 15(2):025212.
- [10] Ishikawa F, Mussler G, Friedland KJ, Kostial H, Hagenstein K, Däweritz L, Ploog KH. Impact of N-induced potential fluctuations on the electron transport in Ga (As, N). Applied Physics Letters, 2005; 87(26):262112.

- [11] Jussila H, Kivisaari P, Lemettinen J, Tanaka T, Sopanen M. Two-Photon Absorption in GaAs_{1- x- y}P_yN_x Intermediate-Band Solar Cells. Physical Review Applied, 2015; 3(5):054007.
- [12] Leibiger G, Gottschalch V, Rheinländer B, Šik J, Schubert M. Model dielectric function spectra of GaAsN for far-infrared and near-infrared to ultraviolet wavelengths. Journal of Applied Physics, 2001; 89(9):4927-4938.
- [13] Lin AS, Wang W, Phillips, JD. Model for intermediate band solar cells incorporating carrier transport and recombination. Journal of Applied Physics, 2009; 105(6):064512.
- [14] López N, Reichertz LA, Yu KM, Campman K, Walukiewicz W. Engineering the electronic band structure for multiband solar cells. Physical Review Letters, 2011; 106(2):028701.
- [15] Luque A, Martí A. Increasing the efficiency of ideal solar cells by photon induced transitions at intermediate levels. Physical review letters, 1997; 78(26):5014.
- [16] Luque A, Martí A, López N, Antolin E, Cánovas E, Stanley C, Diaz P. Operation of the intermediate band solar cell under nonideal space charge region conditions and half filling of the intermediate band. Journal of Applied Physics, 2006; 99(9).
- [17] Marti A, Antolín E, Linares PG, Luque A. Understanding experimental characterization of intermediate band solar cells. Journal of Materials Chemistry, 2012; 22(43):22832-22839.
- [18] Noguchi S, Yagi S, Sato D, Hijikata Y, Onabe K, Kuboya S, Yaguchi H. Analysis of electronic structures of nitrogen δ-doped GaAs superlattices for high efficiency intermediate band solar cells. IEEE Journal of Photovoltaics, 2013; 3(4):1287-1291.
- [19] NSM Archive Physical Properties of Semiconductors, (n.d.). [Online]. Available: http://www.ioffe.ru/SVA/NSM/Semicond/AlGaAs/bandstr.html.
- [20] Okada Y, Morioka T, Yoshida K, Oshima R, Shoji Y, Inoue T, Kita T. Increase in photocurrent by optical transitions via intermediate quantum states in direct-doped InAs/GaNAs strain-compensated quantum dot solar cell. Journal of Applied Physics, 2011; 109(2): 024301.
- [21] Okada Y, Ekins-Daukes NJ, Kita T, Tamaki R, Yoshida M, Pusch A, Guillemoles JF. Intermediate band solar cells: Recent progress and future directions. Applied physics reviews, 2015; 2(2): 021302.
- [22] O'Reilly EP, Lindsay A, Fahy S. Theory of the electronic structure of dilute nitride alloys: beyond the band-anti-crossing model. Journal of Physics: Condensed Matter, 2004, 16(31):S3257.
- [23] Polak MP, Kudrawiec R, Rubel O. Electronic band structure of nitrogen diluted Ga (PAsN): Formation of the intermediate band, direct and indirect optical transitions, and localization of states. Journal of Applied Physics, 2019; 126(17): 175701.
- [24] Ramiro I, Martí A. Intermediate band solar cells: Present and future. Progress in Photovoltaics: Research and Applications, 2021; 29(7):705-713.
- [25] Reason M, Jin Y, McKay HA, Mangan N, Mao D, Goldman RS, Kurdak C. Influence of N on the electronic properties of GaAsN alloy films and heterostructures. Journal of Applied Physics, 2007; 102(10): 103710.
- [26] Shan W, Walukiewicz W, Yu KM, Ager III JW, Haller EE, Geisz JF, Nauka C. Effect of nitrogen on the electronic band structure of group III-NV alloys. Physical Review B, 2000; 62(7):4211.
- [27] Strandberg, R, Reenaas TW. Drift-diffusion model for intermediate band solar cells including photofilling effects. Progress in Photovoltaics: Research and Applications, 2011; 19(1):21-32.
- [28] Suzuki T, Osada K, Yagi S, Naitoh S, Shoji Y, Hijikata Y, Yaguchi H. Molecular beam epitaxial growth of intermediate-band materials based on GaAs: N δ -doped superlattices. Japanese Journal of Applied Physics, 2015; 54(8S1):08KA07.
- [29] Tobías I, Luque A, Martí A. Numerical modeling of intermediate band solar cells. Semiconductor Science and Technology, 2010; 26(1):014031.

- [30] Umeno K, Furukawa Y, Urakami N, Mitsuyoshi S, Yonezu H, Wakahara A. Effects of Mg doping on the electrical and luminescence characterizations of p-type GaAsN alloys grown by MBE. Journal of crystal growth, 2010; 312(2): 231-237.
- [31] Wang QY, Rorison J. Modelling of quantum dot intermediate band solar cells: effect of intermediate band linewidth broadening. IET Optoelectronics, 2014; 8(2):81-87.
- [32] Yagi S, Numata S, Shoji Y, Okada Y, Yaguchi H. Effects of carrier-blocking barrier height on two-step photocurrent generation in dilute nitride intermediate band solar cells. Japanese Journal of Applied Physics, 2023; 62(SK):SK1008.
- [33] Yoshida K, Okada Y, Sano N. Device simulation of intermediate band solar cells: Effects of doping and concentration. Journal of applied physics, 2012; 112(8):084510.

